TIME AND TEMPERATURE INFLUENCE ON THE FAILURE OF TEXTILE COMPOSITES

A. El Mourid[1], R. Ganesan[2], M. Lévesque[1]*
[1] Department of Mechanical Engineering, École Polytechnique, Montréal, Canada,
[2] Department of Mechanical and Industrial engineering, Concordia University, Montreal, Canada
* Corresponding author (martin.levesque@polymtl.ca)

Keywords: *Textile composites, temperature, Aging, damage, tensile tests*

1 Introduction

With the on-going development of high temperature resins, polymer matrix textile composites are increasingly used in hot zones, such as aircraft engines. Specifically, textile composites can be tailored for specific applications by carefully choosing the fabric type (e.g. woven, braided, knitted, etc.) or parameters (e.g. volume fraction, yarns architecture, etc.) to meet loading and environmental conditions. Depending on the loading direction, test temperature and the textile architecture, the ultimate strength may change when compared to that at room temperature. Additionally, long exposures to high temperature, even without loading, can cause degradation in the matrix system due to aging [1]. This phenomenon can further decrease the mechanical strength of the composite material. The aim of this study is to understand the influence of temperature and aging on the failure of braided composites, based on experimental data as well as analytical methods. The first step was the characterization of the composite material using experimental work as well as analytical homogenization. In the second step, an experimental protocol was developed to evaluate the influence of temperature and aging on the behavior of the composite material. Finally, an analysis of the results was preformed to understand the impact of time and temperature on the mechanical properties.

2 Elastic properties of the composite

2.1 Characterization of the composite material

The first step needed to understand the mechanical behaviour of the composite is to properly describe its microstructure. The material studied is a triaxially braided composite embedded in a temperature resistant thermoset matrix. The composite panels were manufactured using a Resin Transfer Molding (RTM) technique. Yarns architecture was obtained using computed micro-tomography, as shown in Figure 1. Table 1 presents the dimensions obtained by the reconstructions of the 3D architecture of the braided composite. The data was then used to build a geometrical representation of the braided geometry, presented in Figure 2. As shown in the figure, direction 1 is along the red yarns, which will be defined as the 0° yarns. Direction 2 is orthogonal to direction 1.

The fibre volume fraction was evaluated to be 56% based on acid digestion tests, and the yarn packing factor was evaluated using image analysis of the polished surface of the yarns. An original picture

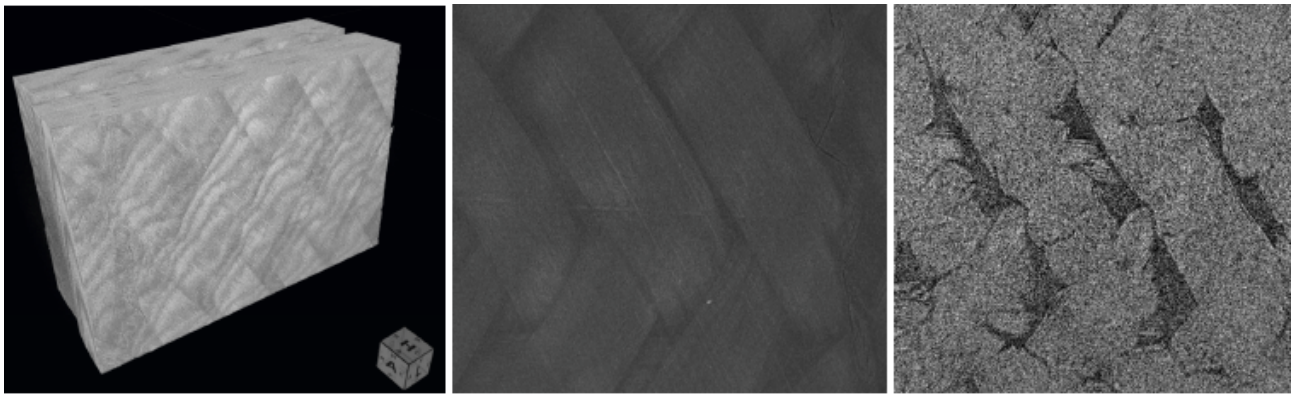

Fig. 1. Micro-tomography images of the triaxially braided textile composite.

was transformed into a biphasic image using a thresholding algorithm, and the pixels representing the fibres were counted and divided by the total number of pixels in the image. The packing factor, representing the volume fraction of the fibres inside the yarns, as well as the fibres and matrix properties, are required for predicting the yarns properties. The yarn-packing factor was evaluated to be 0.71.

2.2 Analytical Homogenization

Due to the presence of matrix inside the yarns, it is necessary to evaluate the yarn properties prior to evaluating the composite's effective properties. An analytical homogenization is performed in this regard. Carbon fibres properties were obtained from manufacturer data and literature [2]. It should be noted that the polymer matrix exhibits viscoelastic response and these properties are that at the steady-state.

All the yarns and composite properties are normalized by the matrix properties at room temperature in the present paper. The yarns effective properties were evaluated according to the methodology of Chamis [3] as:

$$E_{y11} = k_f E_{f11} + (1 - k_f) E_m \quad (1a)$$

$$E_{y22} = E_{y33} = \frac{E_m}{1-\sqrt{k_f}(1-\frac{E_m}{E_{f22}})} \quad (1b)$$

$$G_{y12} = G_{y13} = \frac{G_m}{1-\sqrt{k_f}(1-\frac{G_m}{G_{f12}})} \quad (1c)$$

$$G_{y23} = \frac{G_m}{1-\sqrt{k_f}(1-\frac{G_m}{G_{f23}})} \quad (1d)$$

$$\nu_{y12} = \nu_{y23} = k_f \nu_{f12} + (1 - k_f)\nu_m \quad (1e)$$

$$\nu_{y23} = \frac{E_{y22}}{2\,G_{y23}} - 1 \quad (1f)$$

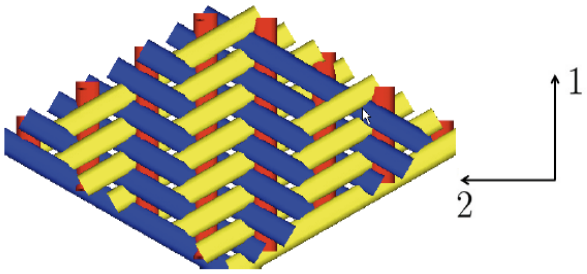

Fig. 2 Architecture of the braided textile composite

where subscript y refers to the yarns, k_f is the packing factor, direction 1 is along the yarns axis while directions 2 and 3 oriented along the transverse directions. This model assumes that the yarns are transversely isotropic, as the carbon fibres. Yarns properties evaluated with Equation (1) are presented in Table 1.

Gommers et al. [4] developed a methodology based on the Mori-Tanaka method to evaluate the mechanical properties of textile composites. In this approach, the yarns geometries are approximated by a series of "divided" inclusions, which are then used in inclusion-based homogenization models for computing the composite's effective properties. The first step consists in defining inclusions that match the yarns geometry. In this work, the yarns cross-sections were assumed to be elliptical. An ellipsoidal inclusion is defined by three characteristic dimensions a_1, a_2 and a_3, as shown in Figure 3. For a prolate spheroid, a_1 defines its characteristic length while a_2 and a_3 define its cross-section. Ratios a_1/a_2, a_2/a_3 and a_1/a_3 are used to compute Eshelby's tensor S [5]. On the one hand, a_2 and a_3 represent the yarn's cross-section. On the other hand, the choice of a_1 is more difficult. In their work, Gommers et al. [4] set a_1 as infinity for simulating yarns' continuity. While this assumption makes sense for long and relatively straight yarns, it loses its validity as waviness increases for high volume fractions. In order to correct this shortcoming, Huysman et al. [6] proposed taking into account the yarn curvature by decreasing the aspect ratio with the following equation:

$$a_1 = \lambda \frac{k}{a_2} \quad (2)$$

where λ is the yarn's local curvature radius and k is a calibration factor. In their paper, Huysman et al. [6] set $k = \pi$. The specific yarns arrangement is then described with a discrete Orientation Distribution Function (ODF). This function is obtained by computing the probability to find each of the inclusions oriented according to specific values of $\{\phi, \theta\}$. For example, if the yarns are divided into 20 ellipsoidal inclusions and if there is only one inclusion oriented according to $\{\phi = 5^\circ, \theta = 88^\circ\}$, then $\{\phi = 5^\circ, \theta = 88^\circ\} = 1/20$. The homogenized response is then evaluated following the equations:

$$\boldsymbol{D} = (\boldsymbol{C_1} - \boldsymbol{C_0}) : \boldsymbol{A} \quad (3a)$$

$$\tilde{C}_{ijkl} = C_{0,ijkl} + \sum_{z=1}^{N} \frac{\rho}{n} a_{mi} a_{nj} a_{ok} a_{pl} D_{mnop} \quad (3b)$$

where $\tilde{C}_{ijkl}$ is the composite's predicted stiffness tensor, $\boldsymbol{A}$ is the so-called 4th order strain localization tensor, ρ the volume fraction of the reinforcing phase, $\boldsymbol{C_1}$ the stiffness of the yarns and $\boldsymbol{C_0}$ the stiffness of the matrix. According to the Mori-Tanaka method, the strain localization tensor $\boldsymbol{A}$ is given by [7]:

$$\boldsymbol{A} = \boldsymbol{T}[\rho_o \boldsymbol{I} + \rho_1 \boldsymbol{T}]^{-1} \quad (4a)$$

$$\boldsymbol{T} = \boldsymbol{I} + \boldsymbol{S} : \boldsymbol{C_0}^{-1}(\boldsymbol{C_1} - \boldsymbol{C_0}) \quad (4b)$$

where ρ_o is the matrix volume fraction, $\boldsymbol{S}$ the Eshelby tensor and $\boldsymbol{I}$ the identity matrix.

Table 2 presents the results of analytical homogenization and comparisons between analytical homogenization and experimental results at 25°C and 225°C. It can be seen that the Mori-Tanaka method delivers more accurate predictions of experimental results when compared to the rule of mixture, and takes into account the decrease of modulus of the matrix at high temperature, which in turn affects the modulus of the composite in both directions.

Three samples cut in direction 1 were tested at 225°C to evaluate the viscoelastic behavior. Creep loads were applied for 20 minutes, followed by recovery periods of 40 minutes. The creep response of the material was negligible. However, there was a relative decrease of 6% in average of the stiffness of the studied composite when the temperature was raised from 25 °C to 225°C.

3 High temperature testing

A triaxially braided (0/±60°) composite material with temperature resistant matrix systems and a service temperature of 225°C was selected to perform tensile tests at different temperatures. The samples were cut in two directions to observe the influence of the loading direction coupled with temperature. Direction 1 is aligned with the warp yarns (0°), while direction 2 is transverse to direction 1, as displayed in Figure 2.

The samples were tested in accordance with the ASTM D3039 [8] standard for tensile tests of composite materials. The tested sample dimensions were 165mm x 25.4mm, which was higher than the minimal required length in the standard. Specimens were tested with and without tabs, to verify the need for tabs. There was no change in the failure mechanisms and ultimate strength, and no gripping induced failure was observed. For the rest of the study, the tabs were removed. The ratio of specimen width to unit cell width was 2.24:1, in accordance with ASTM D6856 [9].

The specimens were tested in an MTS Insight electromechanical testing machine with an environmental chamber. Mechanical grips were used for both room temperature and high temperature tests. The environmental chamber setup was selected to ensure temperature uniformity over the setup. WK type strain gages with a gage length of 12.7 mm were used, so that the gage length was longer than the unit cell. During the tensile tests, the specimens were loaded at a speed of 2 mm/min.

In order to evaluate the damage development during

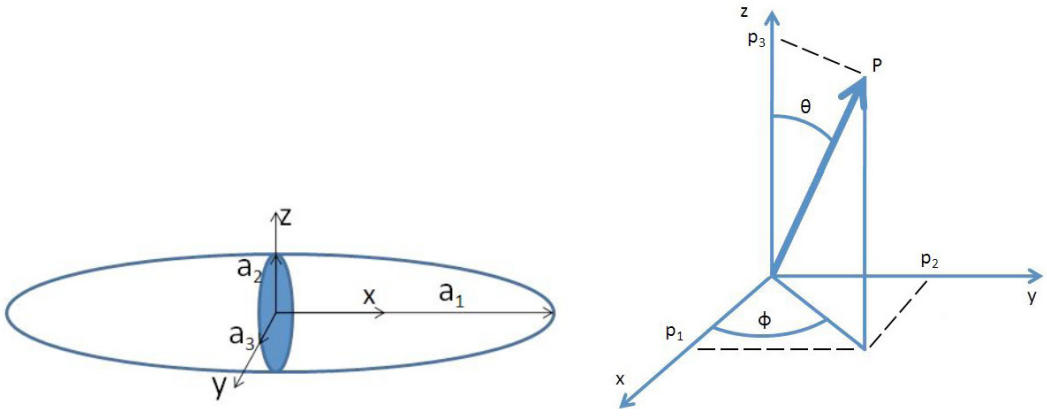

Fig. 3 The geometry of an inclusion is described by three characteristic lengths a_1, a_2 and a_3 and its orientation by Euler angles.

testing, edge replication was performed on some of the tested samples. Edge replication is an established technique used to track cracks in metallography, using replicating film and acetone, or some other precision impression material [10]. While using edge replication, the sample is kept in the testing apparatus. Also, edge replication is a non-destructive characterization technique. In this work, Vinylpolysiloxane was used to create the replicas, for its ease of use when compared to replicating film and acetone. At room temperature, the test was paused at various loads in order to perform the replication. At high temperature, the test was paused and the temperature decreased to around 60 °C. The load was also decreased to 20 % of ultimate tensile strength, in order not to create additional damage during the cooling of the specimen. After the replication, the specimen was heated back, and testing was resumed up to the next load level.

In order to observe the microstructure in the replicas, the edges of the specimen were polished prior to testing [11]. The samples were polished in the first phase with sand paper with finer grit at each step. This phase involved four steps using sand papers of 120, 240, 400 and 600 grit. In the second phase, diamond suspension was used to improve the surface quality. Diamond suspensions of 6 µm, 3 µm and 1 µm were successively used to obtain a mirror polish. In the last phase, an alumina suspension of 0.05 µm was used to provide a final polish and remove the last imperfections. All polishing was performed by hand because of the dimensions of the specimen. This polishing procedure provided the best results in terms of surface quality. Figure 4 shows typical photographs of polished surfaces in directions 1 and 2.

The samples were tested at room temperature and service temperature (225°C), in both directions. Three samples were tested in each condition, for a total of 12 samples for the temperature effects part of the study.

In order to study the influence of aging on the mechanical properties, unloaded composite samples were left in an oven at service temperature for different time periods. A total of 12 samples cut direction 1 were left in the oven for 1 month, 4 months, 12 months and 17 months.

4 Temperature influence on failure

4.1 Macroscopic failure

Differences were observed for the direction of failure, depending on the direction of the loading and temperature. The samples cut along direction 1 samples failed along the ±60° yarns, in a straight line or V-pattern shape, as can be seen in Figure 5. At high temperature, the same failure pattern was observed as can be seen in Figure 6.

For the specimens tested along direction 2, a different failure pattern occurred at high temperature. At room temperature, the failure occurred along the 0° yarns, as shown in Figure 7 However, at high temperature, failure occurred along the 60° yarns as well as 0° yarns, as can be seen in Figure 8.

The main conclusion from these observations is that the yarns loaded by transverse or combined shear/transverse loading will fail first and initiate damage in the composite. Also, the distribution of loading in the yarns changes between room temperature and high temperature. This hypothesis could explain the difference between failure patterns at room temperature and high temperature for samples loaded in direction 2.

4.2 Tensile response curves

Three samples cut in direction 1 were tested at room temperature. Figure 12 displays the stress-strain curves for samples tested in direction 1 (along the 0° yarn), with the results normalized by the ultimate stress and strain of the matrix at room temperature. The curves of response at room temperature show a

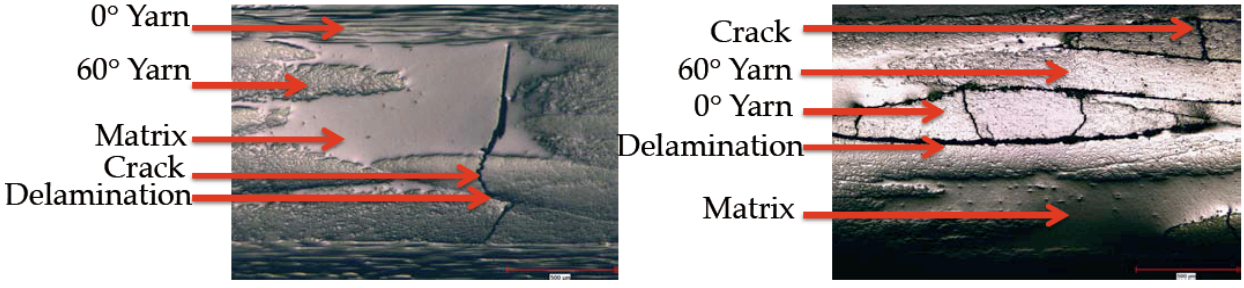

Fig. 4 a) Replica of a sample cut in direction 1 b) Replica of a sample cut in direction 2

bilinear behaviour, with a softening of the composite when the load exceeds 60% of Ultimate Tensile Strength (UTS). At high temperature, the stress-strain curve is almost perfectly linear, with no sign of softening. Also, the ultimate tensile strength is at the same level at room temperature and at high temperature. For the matrix specimens alone, the decrease in UTS strength was close to 45 % between room temperature and high temperature. Because of the yarns at 0° laying in the direction of loading, the decrease in matrix properties had negligible influence on the ultimate failure of the composite.

For the samples tested in direction 2, different observations were made. At room temperature and high temperature, a gradual softening of the composite was observed for increased loading. Figure 12 displays the stress-strain curves for samples tested in direction 2 (orthogonal to the 0° yarns) at room temperature and at 225°C. The first observation is that UTS is 45% higher in direction 2 compared with direction 1 at room temperature. This is explained by the fact that 80% of the yarns lay in ±60° directions. These yarns' load carrying capability is higher in direction 2. Consequently, the Young's modulus in direction 2 is about 54% higher when compared to direction 1. Another interesting observation is that UTS at high temperature was 20 % lower than at room temperature in direction 2, compared with no change in direction 1. This can be explained by the fact that in this direction, the ± 30° yarns relative to direction 2, which provide most of the load carrying capabilities in this direction, are loaded in shear/transverse modes, where the properties of the matrix are critical to the mechanical properties of the composite. In this direction, the degradation of matrix properties because of the temperature had a negative influence on the UTS of the composite.

Table 3 shows Young's modulus and ultimate stress of each of the samples tested at room temperature. The properties are normalized by the matrix properties at room temperature. Table 4 displays the same results at 225°C.

4.3 Edge replication

Edge replication enabled the observation of the microscopic damage evolution and explained some of the failure mechanisms observed on the macroscopic level. At room temperature, a knee point was observed for samples tested in direction 1, at room temperature. This behaviour can be explained with the images provided at 68.5% of UTS by edge replication. At a stress around 68.5% of ultimate stress, transverse cracks appeared in the yarns in the ± 60° direction, as shown in Figure 9. As the load increased, additional cracks in yarns in the ±60° direction as well as matrix cracking occurred in the composite, causing the ±60° direction yarns to lose their ability to carry the load. This is a possible explanation for the decrease in Young's modulus prior to failure. The sample failed following the ±60° yarns, as can be seen in Figure 5. If homogenization is performed without taking into account the yarns at ±60°, the Young modulus of the composite is similar to the one observed after the knee point for the samples tested in direction 1. This further proves that damage is initiated and develops first in the yarns at the ±60° direction for samples loaded in direction 1.

At high temperature, no damage was observed on the ±60° yarns, up to ultimate failure. This observation concurs with the fact that the stress-strain curve is linear until failure at high temperature. The lack of damage in the transverse yarns could be explained by a change in the load distribution at high temperature, with the yarns at 0° carrying most of the load at this temperature. This change in the load distribution would be attributable to a decrease of Elastic properties of the±60° yarns .

For the samples tested in direction 2, different results were observed. As can be seen in Figure 10, transverse cracks in the yarns at the 0° direction appeared at 40% of the ultimate stress at room temperature. As the load increased, a delamination surrounded the 0◦ yarns, which eventually caused the cracks to propagate to the adjacent 60° yarns, causing the final failure of the sample along the 0◦ yarn. The damage evolution recorded with the help of replicas is a confirmation of the damage theory of textile composites presented in the literature [12]. In this direction, the softening is the result of the delamination of the 0° yarn. Using the homogenization models developed in the project, it is possible to evaluate the Young's modulus of the composite in the direction 2, without the influence of the yarns in the 0° direction. The modulus is evaluated at 11 times the matrix's modulus, which is close to the modulus near failure of 11.5.

Similar results were observed for the samples tested at 225°C in direction 2. Figure 11 displays the damage development at high temperature recorded

by edge replication. Transverse cracks in the yarns at the 0° direction appeared at around 25% of ultimate stress, earlier than at room temperature. As the load increased, a delamination surrounded the 0° yarns, which eventually caused the cracks to propagate to the adjacent 60° yarns. A notable difference with the room temperature samples was the extensive delamination of the ± 60° yarns at high temperature and high loads (90% of ultimate stress), as can be seen in Figure 11. The delamination of all the yarns creates two possible paths of failure, seen in Figure 8. The sample failed along the ±60° yarns as well as the 0° yarns. This could be an explanation of the failure at an earlier load for the high temperature specimens.

5. Failure of aged samples

The influence of aging was observed on samples loaded in direction 1. Initially, without aging, UTS was unaffected by high temperature in this direction. However, chemical and physical aging had a detrimental effect on the mechanical properties of the composite. Figure 13 shows the decrease of UTS following aging times of 1 month, 4 months, 12 months and 17 months at 225°C. The test temperature was the same as aging temperature. The results are normalized by UTS of samples prior to aging. During the first month, UTS remained at the same level, as the degradation process didn't start immediately. After one month, the aging process causes a steady degradation in mechanical properties over time.

A closer observation of specimen edges before loading provides insight into the steady drop of ultimate strength. Figures 14 shows microscopic observations of samples edges over various aging times. Before aging, the sample edge is in pristine condition with very few cracks. After one month of aging, small transverse cracks start appearing, as the matrix recedes because of physical aging. After 4 months, cracks develop into the yarns and start causing delamination, increasing the damage state in the composite. After a year, extensive damage can be observed on the specimen edge, with a network of cracks and yarn delamination spanning the entire thickness of the composite samples. These damage mechanisms are very similar to those observed during tensile testing of unaged specimens, although they happen without any loading of the composite.

This degradation is a direct consequence of physical and chemical aging. Physical degradation causes the matrix volume to decrease, creating a stress state because of the presence of the rigid fibres. The matrix shrinkage eventually creates transverse cracks caused by matrix failure inside a yarn. As the aging process increases, the matrix becomes even more brittle, resulting in progression of damage through delamination, creating a network of cracks and delaminations through the composite. This process is further compounded because of chemical aging, which was observed with the help of measurements of mass loss of composite and matrix specimens over time. Chemical aging provokes a degradation of the mechanical properties of the matrix, further decreasing the overall UTS of the composite.

5. Conclusion

The mechanical behaviour of a triaxially braided composite was studied to observe changes caused by temperature and aging. Predictive homogenization tools were used to accurately estimate its elastic properties at room temperature and at high temperature. Test temperature had an influence on the strength of the material, depending on the direction of loading. Specifically, UTS of samples in direction 2, where all yarns are loaded by transverse or shear/transverse combined loading, was lower when compared to room temperature tests.

Aging caused extensive damage to the composite prior to loading. Transverse cracks, followed by delamination of yarns and propagation of cracks resulting in a network of cracks/delamination, were observed as aging progressed in the oven. The development of damage caused a steady decrease in the strength of the composite, with UTS 40 % lower when compared to an unaged specimen after 17 months of aging.

In future works, damage models will be adapted to take into account the influence of temperature and aging on the mechanical properties of textile composites.

References

[1] J. Varghese, J. Withcomb "Micromechanics of oxidation in composites with impermeable fibers". *Journal of composite Materials*, Vol. 43, No. 11, pp 2011-2043, 2009.

[2] R. Maurin, P. Davies, N. Baral, and C. Baley, "Transverse properties of carbone fibres by nano-

indentation and micro-mechanics", *Applied composite materials*, Vol. 15, No.2, pp61– 73, 2008

[3] C. Chamis, Mechanics of composite materials: Past, present and future, *Journal of Composite Technology and Research*, Vol. 11, No. 1,pp3 – 14, 1989

[4] B. Gommers, I.Verpoest, et P.Van Houtte. «The mori-tanaka method applied to textile composite materials». *Acta Materialia*, Vol.46, pp. 2223 – 2235, 1998.

[5] T. Mura, *Micromechanics of Defects in Solids,* Kluwer Academic Publishers, Dordrecht, Netherlands,1982.

[6] G. Huysman, I. Verpoest, P.V. Houtte "A poly-inclusion approach for the elastic modelling of knitted fabric composites", *Acta Materialia,* Vol. 46, pp 3003–3013, 1998.

[7] Benveniste, Y "A new approach to the application of Mori–Tanaka's theory in composite materials", *Mechanics of Materials* Vol. 6, pp 147–157, 1987.

[8] ASTM Standard D3039-08 "Standard test method for tensile properties of polymer matrix composite materials" USA: *ASTM International*, 2008.

[9] ASTM Standard D6856-03 "Standard guide for testing fabric-reinforced textile composite materials", USA: *ASTM International*, 2008.

[10] M. Selezneva, J. Montesano, K. Fawaz, K. Behdinan and C.Poon "Microscale experimental investigation of failure mechanisms in off-axis woven laminates at elevated temperatures". *Composites: Part A*, Vol. 42, pp 1756-1763, 2011.

[11] B. S. Hayes and L.M Gammon, *Optical microscopy of fiber-reinforced composites*, ASM international, 2010.

[12] Dmitry S. Ivanov *, Fabien Baudry, Björn Van Den Broucke, Stepan V. Lomov, Hang Xie, Ignaas Verpoest and K. Current "Failure analysis of triaxially braided composites". *Composites Science and Technology*, Vol. 69, pp 1372-1380, 2009.

Tab. 1. Yarns' mechanical properties and dimensions. The mechanical properties are normalized by matrix properties

$\frac{E_{y11}}{E_m}$	$\frac{E_{y22}}{E_m}$	ν_{y12}	$\frac{G_{y23}}{E_m}$	$\frac{G_{y12}}{E_m}$
58.5	3.45	0.314	3.98	7.23

	Dimension (mm)
Yarn width	2.2
Yarn height	0.21
Distance between 60° yarns	2.7
Distance between 0° yarns	3.4
Yarn fraction at 60°	40 %
Yarn fraction at 0 °	20 %

Tab. 2. Comparison between analytical homogenization and experimental results, at room temperature and high temperature

High temperature (225°C)	Experimental	Mori-Tanaka	Rule of mixtures
E_{11}/E_m	8.7	8.3	10.3
E_{22}/E_m	14.2	13.8	16.5
Room temperature	Experimental	Mori-Tanaka	Rule of mixtures
E_{11}/E_m	9.2	9.6	10.8
E_{22}/E_m	14.6	14.5	17.1

Tab. 3 Tensile testing of the composite at Room temperature.

Direction	$\frac{E}{E_m}$ beginning	$\frac{E}{E_m}$ @ failure	$\frac{\sigma_u}{\sigma_{um}}$
1	9.2	8.1	8.3
2	14.6	11.7	12.3

Tab. 4 Tensile testing of the composite at High temperature (225°C).

Direction	$\frac{E}{E_m}$ beginning	$\frac{E}{E_m}$ @ failure	$\frac{\sigma_u}{\sigma_{um}}$
1	8.7	8.7	8.3
2	14.2	11.5	10.6

Fig. 5. Direction 1 samples after failure at room temperature. The failure line goes along the 60° yarns.

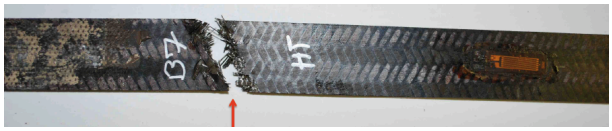

Fig. 6. Direction 1 samples after failure at high temperature. The failure line goes along the 60° yarns.

Fig. 7. Direction 2 samples after failure at room temperature. The failure line goes along the 0° yarns.

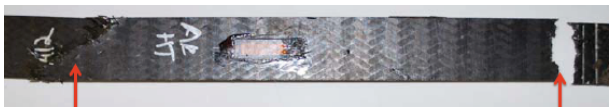

Fig. 8. Direction 2 samples after failure at high temperature. The failure lone goes along the 0° yarns and the 60° yarns.

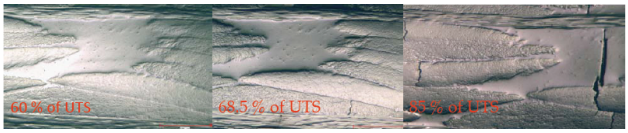

Fig. 9. Replicas at different stress levels at the same location at the edge of a direction 1 sample, tested at room temperature. At 68.5 % of ultimate stress, transverse cracks start appearing on the 60° yarns. At 85 % of the ultimate stress, multiple cracks are visible on the 60° yarns, with matrix cracks visible.

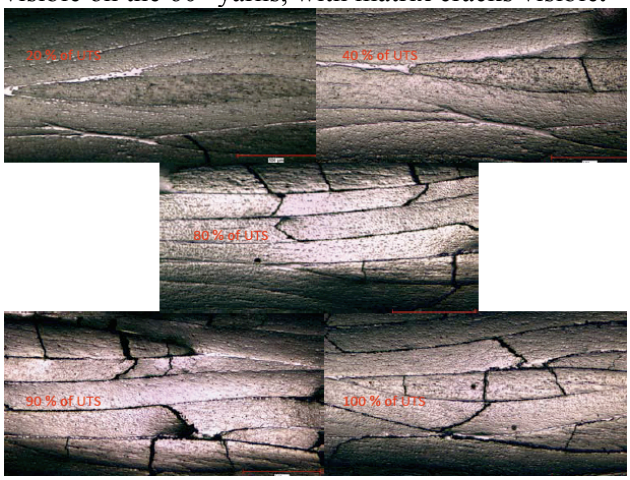

Fig. 10. Replicas at different stress levels at the same location at the edge of a direction 2 sample, tested at room temperature.

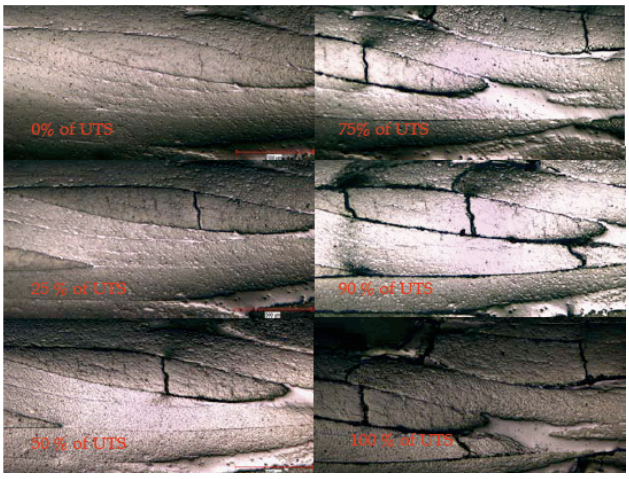

Fig. 11. Replicas at different stress levels at the same location at the edge of a direction 2 sample, tested at high temperature.

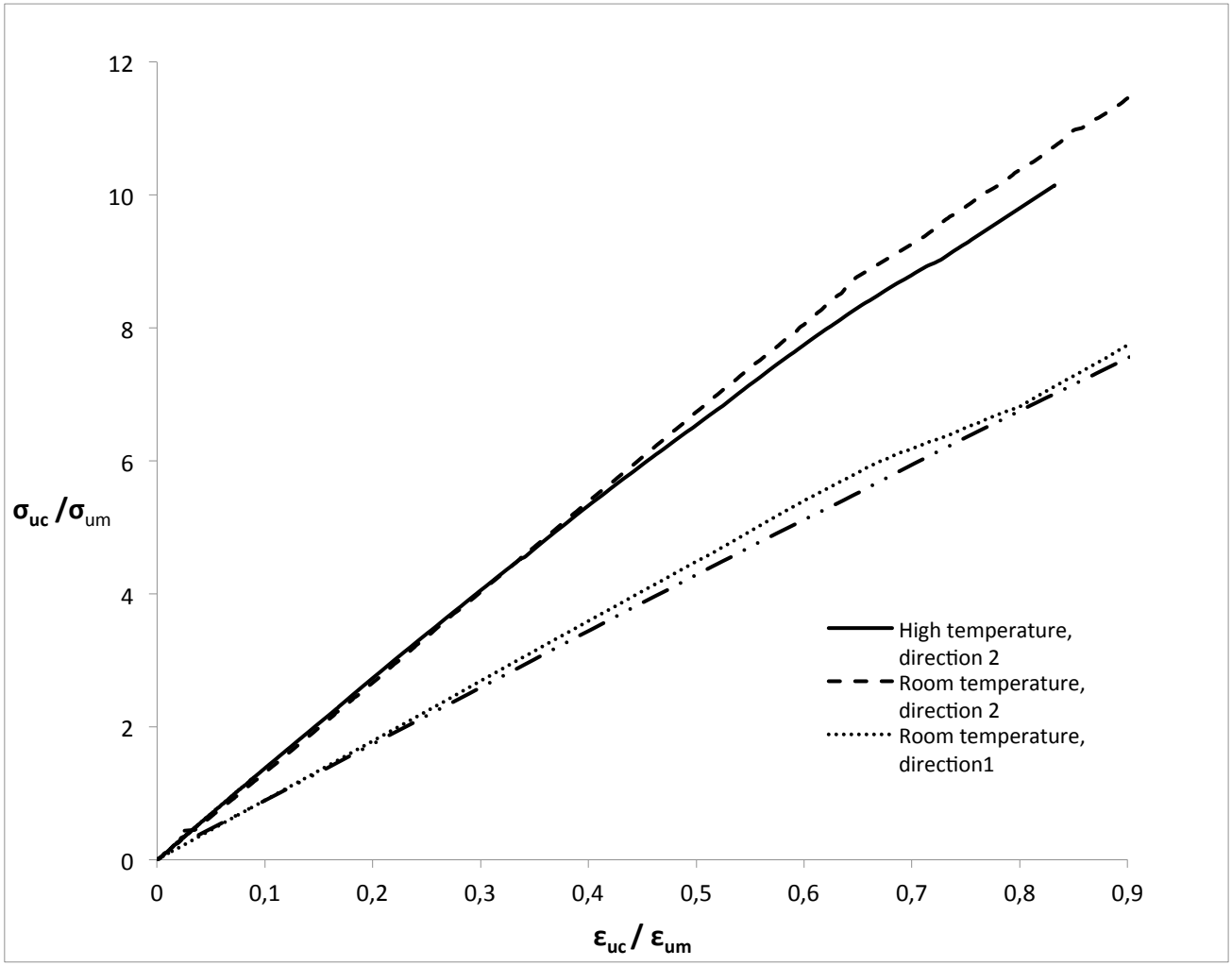

Fig. 12. Tensile curves of samples at room temperature and high temperature

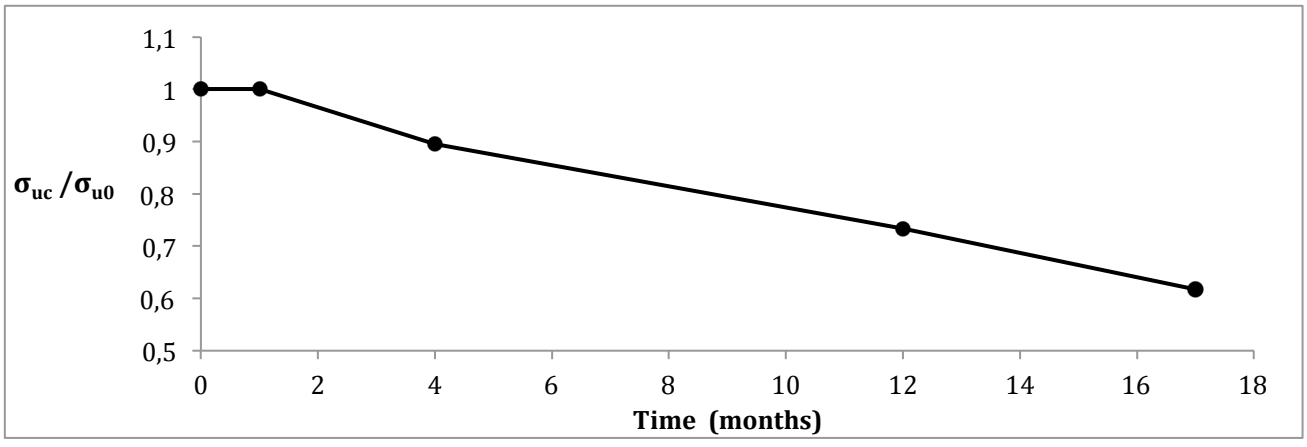

Fig. 13. Ultimate tensile Strength of direction 1 samples after aging at 225°C, normalized by UTS before aging

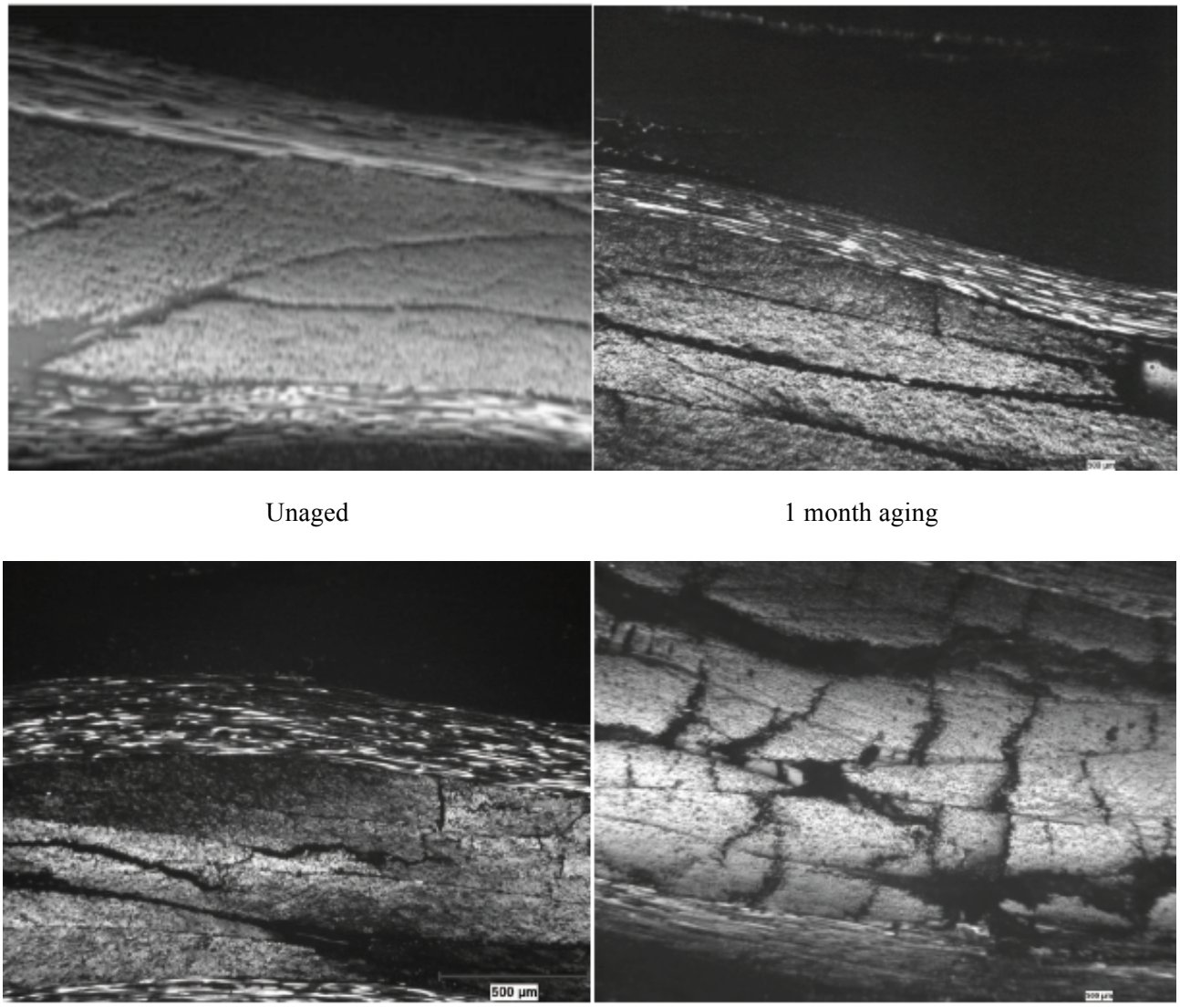

Fig. 14 Microscopic observation of specimen edges at different aging times prior to loading.